VUV Fourier-Transform absorption study of the npπnpπ1Πu-,v,N←X1Σg+,v =0,N transitions in D2

Michèle Glass-Maujean, Ch Jungen, G.D. Dickenson, W Ubachs, N de Oliveira, D Joyeux, L Nahon

HAL Id: hal-01136055
https://hal.sorbonne-universite.fr/hal-01136055

Submitted on 26 Mar 2015

VUV Fourier-Transform absorption study of the $np\pi\ {}^1\Pi_u^-, v, N \leftarrow X^1\Sigma_g^+, v'' = 0, N''$ transitions in D₂

M. Glass-Maujean[1*], Ch. Jungen[2,3], G. D. Dickenson[4],
W. Ubachs[4], N. de Oliveira[5], D. Joyeux[5] and L. Nahon[5]

[1] Sorbonne Universités, UPMC Univ. Paris 06, CNRS, UMR 8112,
Laboratoire d'Etudes du Rayonnement et de la Matière
en Astrophysique et Atmosphères,
F-75005, Paris, France
[2] Laboratoire Aimé Cotton du CNRS, Bâtiment 505
Université de Paris-Sud, F-91405 Orsay, France
[3] Department of Physics and Astronomy, University College London
London WC1E 6BT, United Kingdom
[4] Department of Physics and Astronomy, LaserLaB,
VU University, De Boelelaan 1081,
1081 HV Amsterdam, The Netherlands
[5] Synchrotron Soleil,
Orme des Merisiers, St. Aubin, BP 48,
91192 Gif sur Yvette, France
* phone number: +33(0)-1-4427-4326. e-mail: michele.glass@upmc.fr

March 12, 2015

Abstract

The DESIRS beamline of the SOLEIL synchrotron facility, equipped
with a vacuum ultraviolet Fourier-Transform spectrometer has been
used to measure $Q(N'')$ $(N - N'' = 0)$ absorption transitions of the D₂
molecule. Some 212 Q-lines were assigned and their transition frequen-
cies determined up to excitation energies of 137000 cm⁻¹ above the

ground state, thereby extending the earlier work by various authors, and considerably improving the spectral accuracy (< 0.1 cm^{-1}). The assignments have been aided by first principles multichannel quantum defect theory (MQDT) calculations which also provide predictions of the autoionization widths of the upper levels.

1   Graphical abstract
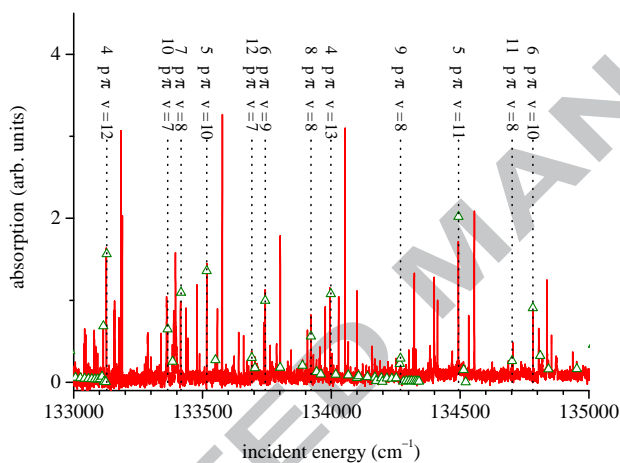
2   Highlights

- 212 photoabsorption transitions to $np\pi$ $^1\Pi_u^-$ upper levels of D$_2$ measured and assigned

- 120 previously unknown spectral lines observed and assigned

- Calculation from first principles of perturbed spectra in D$_2$

- Vibrational progressions followed up to high v in the $np\pi$ Rydberg series ($n = 4 - 14$)

- Quantitative agreement between observations and *ab initio* theory

2

3   Introduction

In this paper we report VUV absorption spectra of molecular deuterium D_2 obtained at the SOLEIL synchrotron facility using the Fourier-Transform technique (DESIRS beamline). These experiments yield precise spectral line positions, with an accuracy of the order of a few hundredths of a cm^{-1}, comparable to the precision achieved in many laser experiments. In contrast to those, however, the Fourier Transform technique is able to produce in a single experiment spectra that cover a large energy domain: the data reported here extend from 118000 to 137000 cm^{-1}, i.e. they cover more than two electron-volts.

We are specifically concerned here with the Q absorption transitions $(N' - N'' = 0)$, which are sharp and primarily populate the levels belonging to various vibrational components of the $np\pi$ Rydberg series with $^1\Pi_u^-$ overall molecular symmetry. These transitions have been studied previously in D_2 by conventional absorption spectroscopy by Monfils [1] for $n = 4 - 5$, and by Takezawa and Tanaka [2] for $n = 4 - 6$, albeit with lower spectral resolution (≈ 0.6 cm^{-1}) than we achieve here. Their data have been conveniently tabulated by Freund, Schiavone and Crosswhite in their report on the spectroscopy of D_2 [3]. The Q transitions to the lowest Rydberg members corresponding to $n = 2$ and $n = 3$ have been studied previously with the synchrotron Fourier-Transform technique [4, 5] so that here, the discussion is limited to principal quantum numbers $4 \leq n \leq 14$.

The analysis of the experimental spectra is greatly facilitated by theoretical calculations. Multichannel quantum defect theory combined with frame-transformation theory and based on quantum defect functions extracted from state-of-the-art potential energy curves is able to produce predictions of excited state $^1\Pi_u^-$ level positions that are accurate to ≈ 1 cm^{-1} throughout. We employ here the formulation of MQDT presented in Ref. [6, 7]. MQDT calculations of the C and D $^1\Pi_u^-$ D_2 excited states have been carried out as early as 1977 [8] and were extended to higher states of the same symmetry later [9].

4   Experimental

The experimental setup has been described in detail by De Oliveira *et al.* [10], while details of its application to the spectroscopy of deuterium were documented by De Lange *et al.* [4] and by Dickenson *et al.* [5]. Four different spectral recordings have been used for the present study. For $E < 119000$ cm^{-1} a spectrum was utilized that had been obtained by crossing the synchrotron ra-

3

diation with an effusive molecular beam. For the range $119000 < E < 131000$ cm^{-1} two overlapping spectra were obtained for a quasi-static gas sample at room temperature employing a T-shaped windowless cell. Finally, for $E > 131000$ cm^{-1}, the windowless cell walls and the inlet port were cooled to liquid-nitrogen temperature providing a quasi-static cooled D_2 sample. The gas pressure in the cell corresponded to ≈ 0.1 mbar. As an example Fig. 1 displays the highest-energy portion of the spectrum obtained between 133000 and 135000 cm^{-1} with the cooled gas sample.
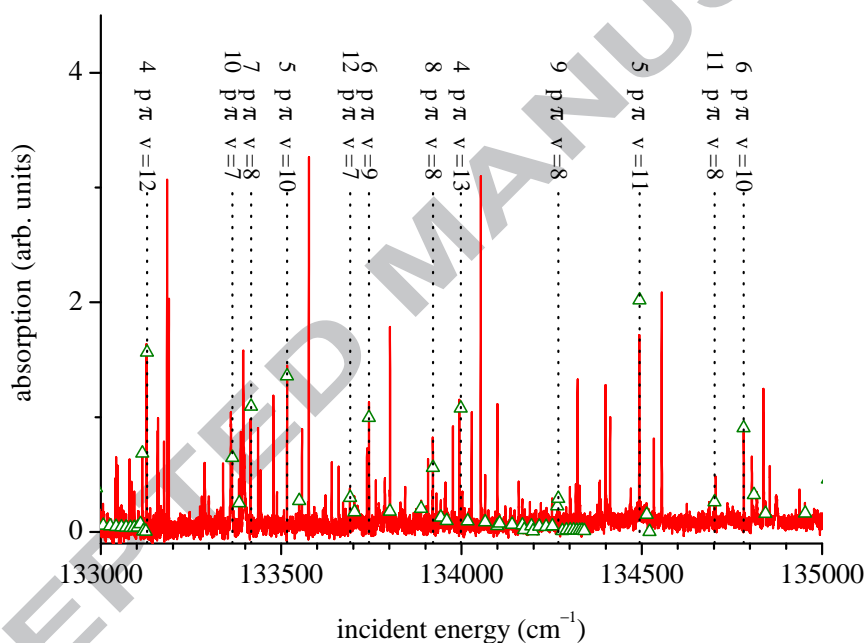
Figure 1.
A section of the D_2 Fourier-transform absorption spectrum recorded at the DESIRS beamline of the SOLEIL synchrotron (continuous trace). Resulting assignments are connected with dotted lines and given at the top. Theoretical positions and intensities of $Q(N'')$ transitions are indicated by triangles.

The Fourier-Transform spectra are intrinsically calibrated by locking and measuring the movement of the travel arm in the FT-instrument by an interferometric measurement with a stabilized helium-neon laser (see Refs. [4, 5] and references therein). A correction of the wavelength/frequency scale must be applied to correct for the slight misalignment of the calibration laser that may be present. We have used the correction determined in Ref. [4] for the

4

jet spectrum and have extrapolated it to higher energies by taking advantage of the fact that the spectra overlap. The uncertainty of the thus determined extrapolated correction has been estimated statistically by examining a large number of observed transitions, and was found to increase with energy as expected: these corrections were: -0.043 ± 0.01 cm^{-1} in the range < 119000 cm^{-1}, -0.018 ± 0.02 cm^{-1}, in the range $119000 < E < 126000$ cm^{-1}, $+0.007 \pm 0.03$ cm^{-1} in the range $126000 < E < 131000$ cm^{-1}, and -0.179 ± 0.035 cm^{-1} at higher energies.

The intensity of the radiation emitted by the undulator has a bell shape as a function of the wavelength that can be approximated by a broad Gaussian with a width of ≈ 6000 cm^{-1}. We have divided the signal corresponding to the transmitted light by this Gaussian in order to obtain I/I_0. Use of Beer-Lambert's law then yields the absorption cross section. However, the strongest peaks absorb nearly 100 % of the radiation so that it is difficult to extract quantitative information on the intensities.

Each observed line profile has been fitted to a Gaussian shape in order to extract its position. The noise level observed in the Fourier-Transform spectra contains a periodic component linked to the spectral resolution and the sinc apparatus function, which imprints an additional uncertainty on the positions of weak spectral lines. The total uncertainty of the line positions is estimated by taking the sum of the uncertainty of the calibration and three times the uncertainty of the Gaussian fit for each line. For the weakest transitions an extra contribution is added accounting for the effect of the periodic noise.

5 Theory

Our spectral analysis is based on theoretical multichannel quantum defect theory (MQDT) calculations. This approach has two principal features: First, conventional quantum-chemical clamped-nuclei potential energy curves $U_{n\Lambda}(R)$ of given symmetry Λ and for low n principal quantum numbers, such as available in the literature ($^1\Pi_u$ for $n = 2 - 4$ in the present case [11, 12]), are converted into clamped-nuclei quantum defects $\mu^{(\Lambda)}(E, R)$ by straightforward use of the Rydberg equation. These turn out to be only weakly dependent on n - and hence of a more universal nature than the underlying individual potential energy curves (PEC's) - so that higher $n-$members and even continuum electron phase shifts $\pi\mu^{(\Lambda)}(E, R)$ can be reliably predicted by extrapolation. Rovibrational motion is taken into account by means of a frame transformation which involves evaluating integrals over the vibrational degree of freedom of the type $\langle v^+ N^+ | \mu^{(\Lambda)}(E, R) | v^{+'} N^{+'} \rangle$ where $v^+ N^+$ denote

5

the vibrational-rotational wavefunctions of the D_2^+ 'target' ion core. For $v \neq v'$ these integrals provide the desired information about non-adiabatic processes, such as vibronic coupling among Rydberg states or vibrational autoionization $nv \rightarrow \epsilon v'$, where n refers to an 'initial' Rydberg state subject to autoionization, and ϵ to the 'final' ionization continuum. The basis of this approach has been reviewed [13, 14], while the practical details of the present somewhat simplified application are given in Refs. [6, 7]. By and large, the simplified approach applied to the absorption spectrum of diatomic hydrogen is known to yield excited rovibronic level positions to better than 1 cm^{-1} - generally sufficiently accurate to make reliable assignments. Fig. 1 includes calculated $Q(N'')$ transitions and demonstrates how the assignments are made. As we shall discuss in Sec. 8, the simplified MQDT approach tends to give poorer results for high vibrational quantum numbers as some of the assumptions underlying it start to break down.
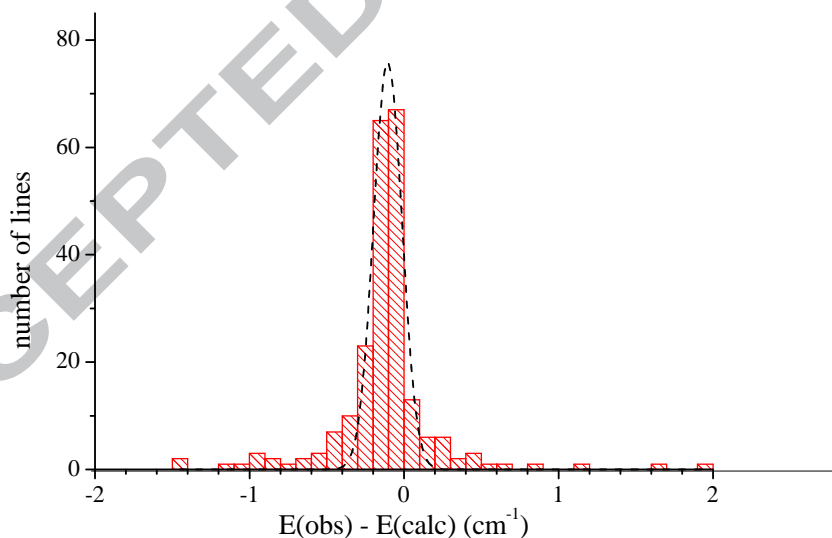
6 Results

Figure 2.
Histogram showing the distribution of deviations observed-calculated for 212 $Q(N)$ transitions. The dashed line represents a Gaussian fit of the distribution resulting in a width of 0.18 cm^{-1} and a displacement of -0.10 cm^{-1}.

The Q transitions leading to the $3p\pi\,^1\Pi_u^-$ upper state have been published previously [5] and are not discussed here. Tables 1 and 2 contain our measurements and assignments from $n = 4$ up to $n = 14$. Fig. 2 is a histogram displaying the deviations observed - calculated for all 212 Q transitions corresponding to $n \geq 4$ that we have observed and assigned. The mean deviation amounts to -0.10 cm^{-1}, while the width at half-maximum is 0.18 cm^{-1}. There is a number of outliers as well, which will be discussed in the following subsections where the results are presented in more detail for the individual electronic states.

6.1 The $4p\pi D'\,^1\Pi_u^-$ state
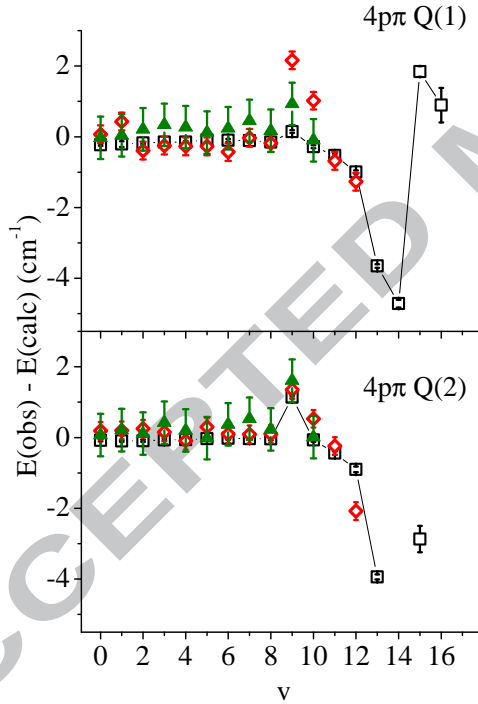
Figure 3.
Deviations observed-calculated for the $Q(1)$ (top) and $Q(2)$ (bottom) lines of the $4p\pi D'$ $^1\Pi_u^- \leftarrow X^1\Sigma_g^+$ transition in D$_2$, plotted as function of the vibrational quantum number. Open squares (black): present measurements - present MQDT calculations. Triangles (green): Takezawa and Tanaka [2] - MQDT. Open diamonds (red): Roudjane *et al.* [15] - MQDT. The error bars correspond to the experimental uncertainties. In the case of the present experiments they are for the most part smaller than the size of the symbols.

7

The Q transitions leading to the $n = 4$ Rydberg member, $4p\pi$, have previously been measured by Monfils [1] and Takezawa and Tanaka [2] in absorption and by Roudjane *et al.* [15] in emission. Fig. 3 consists of a set of plots of the deviations E(observed) - E(calculated), in cm^{-1}. These show the deviations for the $Q(1)$ and $Q(2)$ transitions as functions of the vibrational quantum number v. The corresponding information extracted from the data of Refs. [2] and [15] is also included in the figure. It may be seen that to within the experimental uncertainties, corresponding to 0.6 cm^{-1} for Ref. [2] and to 0.25 cm^{-1} for Ref. [15] - i.e. larger than the present uncertainties - the old and the new sets of data are by and large consistent.

Figure 4.
Absorption spectrum of D$_2$ near 130170 cm^{-1}, recorded with the VUV Fourier-Transform spectrometer. The position and intensity of the $4p\pi, v = 9$ $Q(1)$ peak calculated by MQDT are indicated by a triangle with associated dashed vertical line. The assignment made by Roudjane *et al.* [15] is also indicated. See Ref. [16] for the assignment of the $R(1)$ transition which is also indicated, and further below in this Section for the Hund's case d notation used for that assignment.

A few exceptions also occur, however:

- $Q(1), v = 9$: the present transition frequency measurement yields the value 130168.41 ± 0.04 cm^{-1} whereas Ref. [15] gives 130170.44 cm^{-1} at a position where no absorption occurs in the present spectrum (see Fig.

8

4). We suspect that the assignment made in Ref. [15] was erroneous. Ref. [2] reported the value 130169.2 ± 0.6 cm^{-1} for the same transition. However, we find that there are in fact two spectral lines, one at 130168.41 cm^{-1}, which we have assigned as $4p\pi, v = 9$ $Q(1)$, and one at 130169.68 cm^{-1}, which we have assigned as $14p3, v = 4$ $R(1)$ [16]. These lines were not resolved in the earlier studies.

- $Q(2), v = 12$: Ref. [15] reports the value 133041.09 for this transition whereas we find 133042.34 cm^{-1}. We suspect that the uncertainty of their measurement was underestimated by the previous authors in this case. Specifically, the following situation occurs near the expected
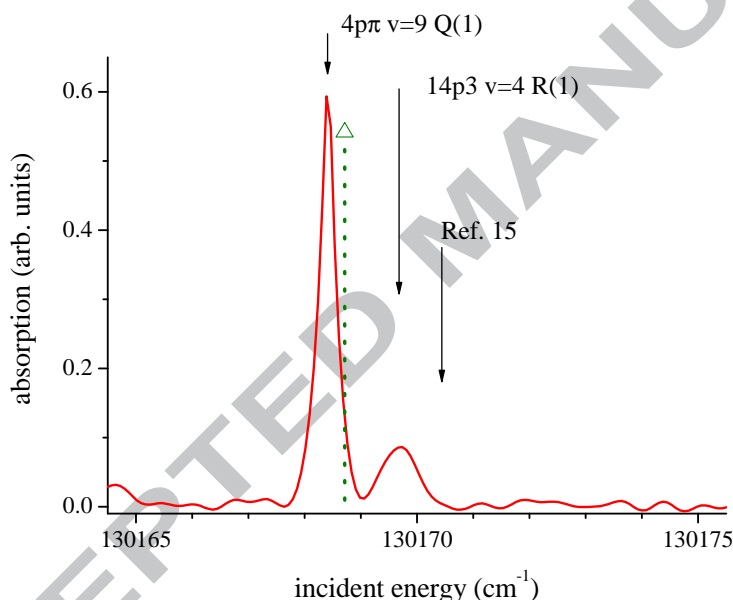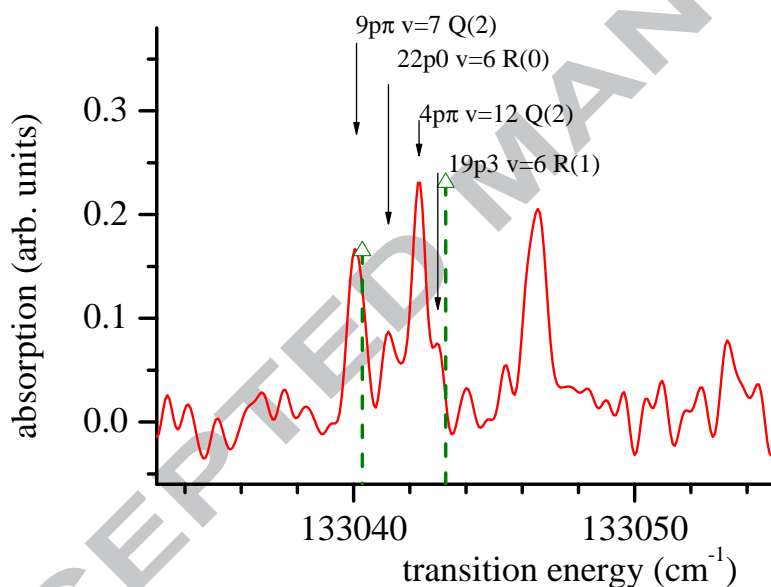

Figure 5.

Absorption spectrum of D$_2$ near 133040 cm^{-1}, recorded with the VUV Fourier-Transform spectrometer. The arrows point to the experimental peak positions, whereas the triangles with dashed lines correspond to the MQDT predictions of $Q(2)$ transitions (see text for more details and Ref. [16] for the assignments of the $R(0)$ and $R(1)$ transitions).

position of the $Q(2)$ transition to the $4p\pi, v = 12$ upper level: a quadruplet of close lying lines is observed as shown by Fig. 5. The MQDT calculations predict the following positions (in cm^{-1}) and Einstein A

9

coefficients (in units of 10^5 s^{-1}):

$$
\begin{array}{lll}
Q(2) \quad 9p\pi, v = 7: & 133040.20 & 16 \\
R(0) \quad 22p0, v = 6: & 133041.45 & 5 \\
R(1) \quad 19p3, v = 6: & 133042.84 & 3 \\
Q(2) \quad 4p\pi, v = 12: & 133043.23 & 23
\end{array}
$$

(where npN^+ replacing $np\lambda$ corresponds to Hund's case d notation appropriate for high-n states, see [14]). Taking account of the population of the ground state rotational levels at 78 K one thus expects the intensity ratios 1.6/0.5/0.3/2.3 for the four lines (in the order as given above). Based on these considerations we make the following assignments of the observed quadruplet of lines (intensities in arbitrary units):

$$
\begin{array}{lll}
Q(2) \quad 9p\pi, v = 7: & 133040.10 & 12 \\
R(0) \quad 22p0, v = 6: & 133041.24 & 6 \\
Q(2) \quad 4p\pi, v = 12: & 133042.34 & 15 \\
R(1) \quad 19p3, v = 6: & 133042.98 & 3 \; .
\end{array}
$$

These assignments do not quite agree with those made in Ref. [15] for the same group; it appears in particular that $9p\pi, v = 7$ and $4p\pi, v = 12$ were not resolved in the earlier experiment.

Our measurements enable us to assign the $4p\pi$ progression of $Q(1)$ and $Q(2)$ transitions up to $v = 16$. The deviations observed-calculated between the measurements and the MQDT calculations are in general smaller than ≈ 0.2 cm^{-1}, whereas they increase up to several cm^{-1} for $v \geq 12$. $Q(2), v = 14$ has not been identified and is probably even more strongly perturbed. It therefore appears that our calculations, which are limited to channels derived from the np manifold of states, miss additional channel interactions which become effective above about 130400 cm^{-1}. These are probably also at the origin of the jump that occurs for $Q(2), v = 9$ in Fig. 3.

6.2 The $5p\pi$ $^1\Pi_u^-$ state

The vibrational progression of Q transitions leading to the $5p\pi$ state of D$_2$ has previously been followed up to $v = 5$ by Takezawa and Tanaka [2]. In the present work we have been able to extend the measurements of the $Q(1)$ and $Q(2)$ transitions up to $v = 12$ with significantly increased precision. The

10

Figure 6.
Deviations observed-calculated for the $Q(1)$, $Q(2)$ and $Q(3)$ transitions to the $5p\pi D''$ $^1\Pi_u^-$ upper state in D_2, plotted as function of the vibrational quantum number. The symbols have the same meaning as in Fig. 3.

$Q(3)$ and $Q(4)$ transitions are rather weak in absorption by the 78 K gas sample, so that the observations are limited to lower v values.

Fig. 6 is a plot of the deviations observed - calculated versus the vibrational quantum number for the $Q(1)$, $Q(2)$ and $Q(3)$ transitions. Our values are represented by squares while those from Ref. [2] are represented by triangles. It may be seen that the two sets of data are consistent wherever data from Ref. [2] are available, with the sole exception of $Q(2), v = 0$ where the earlier assignment is probably erroneous due to spectral overlapping which could not be resolved at the time. Overall, the deviations observed - calculated obtained in the present work are smaller than about 0.3 cm^{-1}, with just a few exceptions: deviations larger than 0.3 cm^{-1} but still smaller than

11

1 cm^{-1} appear for $Q(1), v = 11$ and $Q(2), v = 8$. A substantially larger deviation occurs for $Q(2), v = 3$. In that case we clearly observe two lines placed symmetrically on either side of the calculated position, but we have not been able to assign the perturber level. Systematic deviations appear also in the $Q(2)$ series for the highest v values. It is likely that, as for $4p\pi$, these deviations are due to shortcomings of our calculations which do not yet include the f−type channels and do not explicitly account for core excited channels. The transitions $Q(3)$ $v = 4$ and 5 are too weak in our spectra to be measured.

6.3 The $6p\pi$ $^1\Pi_u^-$ state
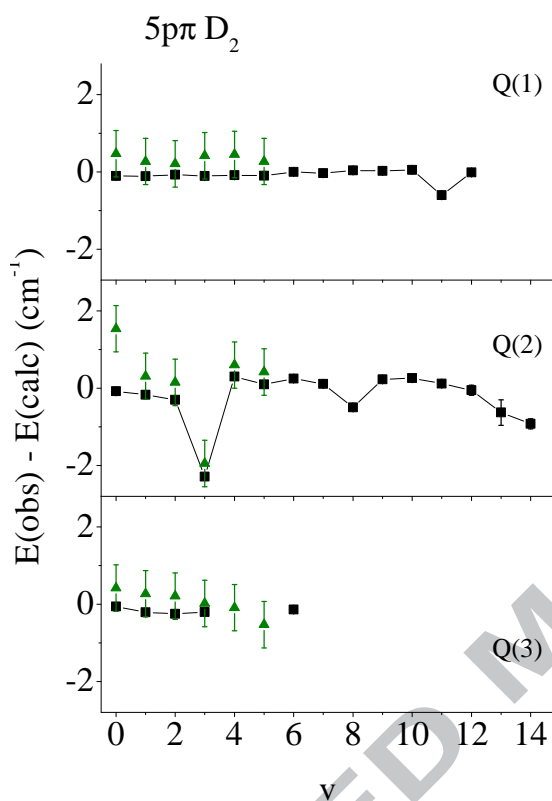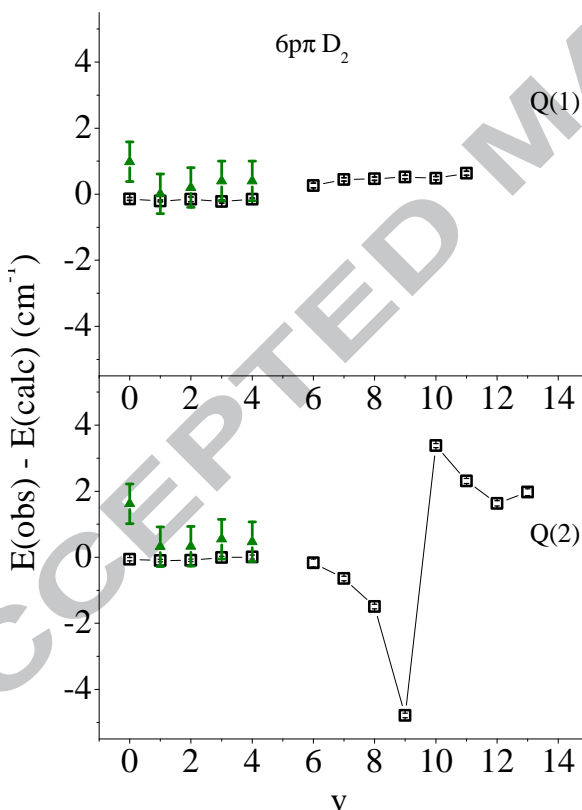

Figure 7.
Deviations observed-calculated for the $Q(1)$ and $Q(2)$ transitions to the $6p\pi$ $^1\Pi_u^-$ upper state in D$_2$, plotted as function of the vibrational quantum number. The symbols have the same meaning as in Fig. 3.

The spectra obtained at SOLEIL have enabled us to extend the assignments of the $6p\pi$ state vibrational structure up to $v = 11$ for the $Q(1)$ transitions and up to $v = 10$ for the $Q(2)$ transitions as compared to $v = 4$ in the earlier work [2], with significantly increased precision at present. Fig. 7 displays the deviations observed - calculated for this state. The disagreement between the earlier [2] and the present values for $Q(1)$ and $Q(2)$ $v = 0$ is surprising and might possibly be due to a misprint in the earlier paper.

The deviations observed - calculated for the $6p\pi$ levels are in line with those obtained for $4p\pi$ and $5p\pi$. They amount to a fraction of a wavenumber unit in many cases, but a spectacular exception occurs for $Q(2)$, $v = 7$ to 10, where the deviations exhibit the effects of an anticrossing with an as yet unknown level, and jump from -4.8 to +3.4 cm^{-1} between $v = 9$ and 10. Surprisingly, this perturbation is not visible in the $Q(1)$ vibrational progression where the deviations observed - calculated remain small and smooth throughout.

Our calculations predict that the $Q(1)$ and $Q(2)$ transitions corresponding to $v = 5$ should have intensities about 1/40 th of their $v = 4$ counterparts; we have indeed not been able to extract their positions from the experimental noise. Our calculations indicate that the $Q(2)$, $v = 3$ line is embedded in the dense manifold of high-n Rydberg levels converging to the $v^+ = 1, N^+ = 2$ threshold and via vibronic interaction with those forms a 'complex' resonance. This is illustrated by Fig. 8 which shows that the calculated overall width of the 'complex' resonance is smaller than the Doppler width of our experiment, with the result that its fine structure is not resolved in the present experimental spectrum.

6.4 The $np\pi$ $^1\Pi_u^-$ series with $n \geq 7$

In all we have been able to assign 52 $Q(1)$ lines and 48 $Q(2)$ lines corresponding to $n \geq 7$. This is somewhat surprising since at room temperature the population of the $N'' = 2$ ground state rotational level is twice that of the $N'' = 1$ level so that one would expect $Q(2)$ transitions to be more easily observable than $Q(1)$ transitions. On the other hand, only a single $Q(3)$ transition with $n = 7$, and no $Q(4)$ and $Q(5)$ lines at all with $n > 6$ could be detected in our spectra.

7 Line widths

The observed linewidths correspond to the sum (convolution) of three effects: (i) the apparatus function which accounts for 0.16 cm^{-1} in the present mea-
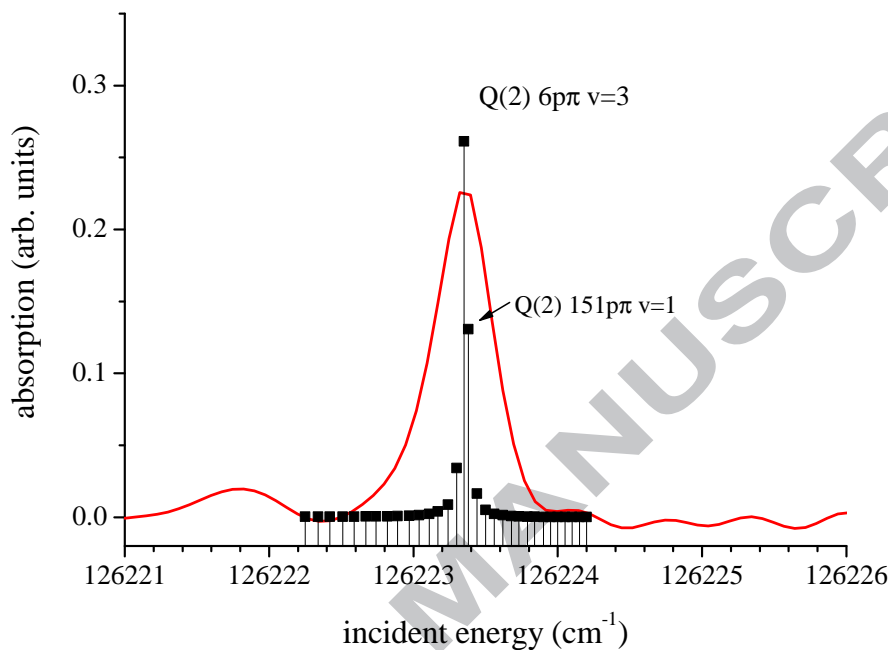
Figure 8.

Absorption spectrum of D_2 near 126220 cm^{-1}, recorded with the VUV Fourier-Transform spectrometer, near the $6p\pi, v = 3$ $Q(2)$ transition. The spectrum calculated by MQDT is also indicated (squares) and shows that the transition is in fact a 'complex' resonance. The ionization limit corresponding to $v^+ = 1, N^+ = 2$ is situated at 126228 cm^{-1}, higher than this resonance.

surements (a sinc-function of 0.16 cm^{-1} width related to the settings and travel arm of the FT-instrument), (ii) the Doppler width which corresponds to a Gaussian and varies depending on the spectral recordings as detailed in Ref. [4], and (iii) the natural profile of each excited level which essentially is a Lorentzian arising from the fluorescence, dissociation and/or ionization decay processes.

We have calculated the line profile resulting from the convolution of the (known) Gaussian representing the effective Doppler width (including the width resulting from the inhomogeneously distributed outward diffusing gas in the cooled T-shaped cell, as well as a small additional broadening due to possible beam pointing instability during the FT-recordings) and the (unknown) Lorentzian corresponding to the natural width. The result of the convolution was fitted itself by a Gaussian, which then was compared to the

14

experimentally determined effective width. We varied the assumed natural width for each transition until the observed effective width could be reproduced. The uncertainty of the thus determined natural width was taken to be three times the uncertainty obtained in the fit. This procedure has been applied to the identified $Q(1) - Q(3)$ transitions appearing with sufficient intensity at energies above 125000 cm^{-1}.

Fluorescence constitutes the only open decay channel for energies lower than 119000 cm^{-1}, while in the range from 119000 to 125000 cm^{-1} dissociation may also occur. Ionization on the other hand sets in above 125000 cm^{-1}. We know from H$_2$ that molecular dissociation can hardly compete with molecular fluorescence in the levels excited by the Q transitions [17]. We may therefore be certain that this is even less the case in the heavier system D$_2$ where dissociation is yet slower. The intensity calculations further indicate that molecular fluorescence takes place on a time scale ≥ 7 ns for $n \geq 4$, corresponding to widths ($\approx 7 \cdot 10^{-4}$ cm^{-1}) again far less than the autoionization widths. Therefore autoionization alone should fully account for our observations in the present situation. We have consequently used MQDT to evaluate the ionization partial widths (autoionization), while neglecting the contributions due to predissociation and photon emission.

Fig. 9 displays the observed and calculated widths of the $Q(2)$ transitions plotted as functions of the transition energy. It turns out that in the vast majority of cases the natural widths, determined from experiment by the procedure outlined above and represented by filled squares with error bars, are smaller than their uncertainties. There are only four exceptions, which all correspond to $Q(2)$ lines, namely $9p\pi, v = 4$, $12p\pi, v = 4$, $10p\pi, v = 6$ and $10p\pi, v = 7$ (cf. the figure). Fig. 9 demonstrates that the calculated autoionization widths, represented in the plot by open squares, are fully compatible with the experimental determinations despite the fact that in most cases we are not able to determine more than an upper limit of the natural width. The calculated widths are for the most part very small, $\approx 1 \cdot 10^{-3}$ cm^{-1}, and difficult to extract with good numerical precision, and therefore we do not give their values here in tabular form.

Fig. 9 further shows that the widths of the four $Q(2)$ transitions mentioned above which are significantly broader than the effective Doppler width, are also satisfactorily reproduced by the theory, with calculated values of 0.35, 0.14, 0.36 and 0.42 cm^{-1}, respectively. These four cases correspond to transitions $np\pi, v$ that appear just above the $v - 1$ ionization limit so that they may autoionize by a $\Delta v = 1$ process, known to vastly dominate over $\Delta v > 1$ processes [18, 19] which would be possible *below* the $v - 1$ threshold. They are further favored by the $(n^*)^{-3}$ rule which suppresses autoionization in the *higher n* Rydberg members [20]. A further condition for autoionization

15
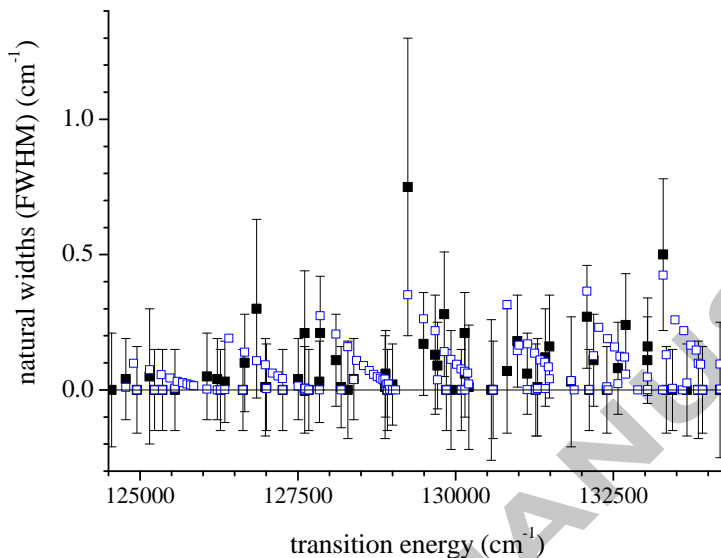
Figure 9.

Natural widths of $Q(2)$ transitions in D_2 plotted as function of the transition energy. The filled squares with error bars are observed values obtained by deconvolution from the apparatus width and Doppler width as described in the text. The open squares are autoionization widths calculated by MQDT. Only four lines have measured widths larger than the uncertainty 0.17 cm^{-1} of the deconvolution process. These correspond to $9p\pi, v = 4$, $10p\pi, v = 6$, $8p\pi, v = 7$ and $10p\pi, v = 7$, respectively, in agreement with the calculations.

widths to be determinable in the present context is that the Q transitions must be sufficiently strong. Our calculated intensities are indeed compatible with the observed strong intensities for all four transitions discussed here - we have previously shown [6] that Q transitions with $^1\Pi^-$ upper state symmetry, while subject only to basically weak vibronic coupling, often exhibit surprisingly strong intensity perturbations.

8   Discussion

The present work considerably extends the knowledge of the $^1\Pi_u^-$ excited states of the D_2 molecule beyond what was known through the early work of Monfils [1] and Takezawa and Tanaka [2, 3]. Specifically it has been possible to extend the observations to higher vibrational quantum numbers up close to

16
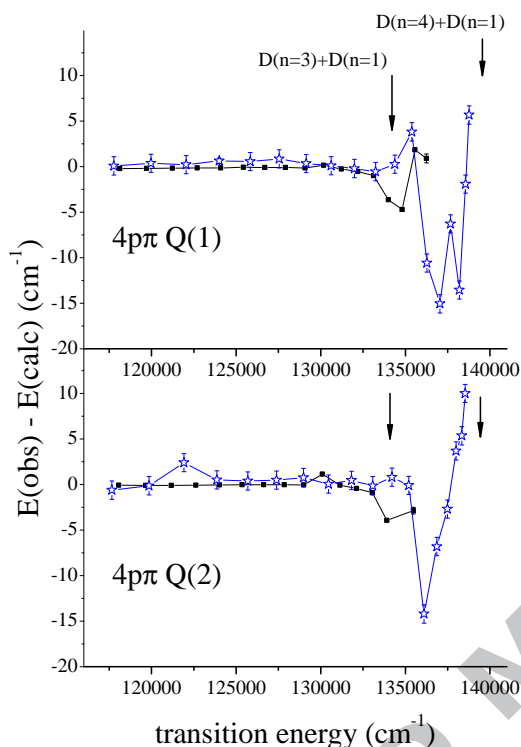
Figure 10.

Deviations observed-calculated for the $Q(1)$ (top) and $Q(2)$ (bottom) lines of the $4p\pi D'\ ^1\Pi_u^- \leftarrow X^1\Sigma_g^+$ transition of D_2 and H_2, plotted as functions of the total energy. Full squares: present measurements - present MQDT calculations. Stars: deviations for H_2 (Ref. [7] and Glass-Maujean *et al.* unpublished). The arrows indicate the positions of the $D(1s) + D(n = 3)$ and $(n = 4)$ dissociation limits, respectively.

the $D(1s)+D(n = 4)$ dissociation limit. Further, the use of the VUV Fourier-Transform spectrometer at the SOLEIL synchrotron facility has enabled the accuracy to be improved considerably, namely to ≈ 0.03 cm^{-1} for the lower transitions and to ≈ 0.30 cm^{-1} for the shortest-wavelength transitions.

The MQDT approach [6, 7] which we have used previously with success for H_2, has been instrumental in D_2 for the purpose of identifying the Q transitions in the rich absorption spectrum, which is a many-line rather than a band-type spectrum. While the success of the approach is not really unexpected and indeed extremely helpful, as it has allowed us to predict the vast majority of the Q transitions correctly to within ≈ 0.1 to 0.2 cm^{-1} - cf. the histogram of Fig. 2 - its shortcomings are in a sense more interesting as they point to necessary future developments. In Fig. 10 we have plotted the

17

deviations experiment - theory for the $4p\pi$ Q transitions both for H_2 and D_2 as functions of the total energy instead of the vibrational quantum number as in Fig. 3. The plots demonstrate that the behavior in D_2 parallels that in H_2. Fig. 10 thus reveals the interesting fact that the (relatively mild) breakdown of the MQDT version used in the present work takes place at the same energy both for H_2 and D_2, near 136000 cm^{-1}, substantially below the $D(1s)+D(n=4)$ dissociation limit at 139600 cm^{-1}.

We recall here that the present MQDT approach is based on the clamped nuclei $^1\Pi_u$ quantum-chemical potential energy curves computed by Wolniewicz and Staszewska [11, 12] for $n = 2-4$ which it uses to extract quantum defect functions which then are extrapolated to higher energies. The point to be noted is that for $n = 2$, 3 and 4 the $np\pi$ $^1\Pi_u$ Rydberg states of diatomic hydrogen do not change the principal quantum number value upon dissociation, that is they correspond to *unpromoted* Rydberg orbitals in the terminology of Mulliken [21]. This is however no longer the case for higher n-values. For instance the $5p\pi$ Rydberg state dissociates into $H(1s)+H(n=4)$ (see Fig. 1 of Ref. [22] and the accompanying discussion), which means that it is *singly promoted*. According to Mulliken [21] this type of change reveals the onset of what he called *major configuration mixing* (major CM), arising from the fact that at large internuclear distance the electronic wavefunction cannot even approximately be represented by a single core state with an attached Rydberg electron, requiring instead an equal mixture of ground state core and core excited Rydberg configurations. In the case of the $np\pi$ Rydberg states this change occurs near an energy not far from the $H(1s)+H(n=4)$ dissociation asymptote [22], in agreement with what the present Fig. 10 indicates. This physics must be built into the MQDT formalism as well, by explicit inclusion, first, of higher-ℓ partial waves, and, second, of core-excited channels in addition to the channels associated with the ground state core. Work in this direction is underway.

9 Acknowledgments

References

[1] A. Monfils, J. Mol. Spectrosc. **15**, 265-307 (1965).

[2] S. Takezawa and Y. Tanaka, J. Mol. Spectrosc. **54**, 379-401 (1975).

[3] R. S. Freund, J. A. Schiavone, and H. M. Crosswhite, J. Phys. Chem. Ref. Data **14**, 235-283 (1985).

[4] A. de Lange, G. D. Dickenson, E. J. Salumbides, W. Ubachs, N. de Oliveira, D. Joyeux and L. Nahon, J. Chem. Phys. **136**, 234310-1 - 234310-9 (2012).

[5] G. D. Dickenson, T. I. Ivanov, W. Ubachs, M. Roudjane, N. de Oliveira, D. Joyeux, L. Nahon, W.-Ü. L. Tchang-Brillet, M. Glass-Maujean, H. Schmoranzer, A. Knie, S. Kuebler and A. Ehresmann, Mol. Phys. **109**, 2693-2708 (2011).

[6] M. Glass-Maujean and Ch. Jungen, J. Phys. Chem. **A113**, 13124-13132 (2009).

[7] M. Glass-Maujean, Ch. Jungen, M. Roudjane and W.-Ü. L. Tchang-Brillet, J. Chem. Phys. **134**, 204305-1 - 204305-14 (2011).

[8] Ch. Jungen and O. Atabek, J. Chem. Phys. **66**, 5584-5609 (1977).

[9] S. C. Ross and Ch. Jungen, in: XVth International Conference on High Resolution Infrared Spectroscopy, Prague, Czech Republic, 1998, abstract D46 [http://www.chem.uni-wuppertal.de/conference/].

[10] N. de Oliveira, M. Roudjane, D. Joyeux, D. Phalippou, J. C. Rodier, and L. Nahon, Nature Photon. **5**, 149-153 (2011).

[11] L. Wolniewicz and G. Staszewska, J. Mol. Spectrosc. **220**, 45-51 (2003).

[12] http://fizyka.umk.pl/ftp/pub/publications/ifiz/luwo (2013).

[13] C. H. Greene and Ch. Jungen, Adv. At. Mol. Phys. **21**, 51-121 (1985).

19

[14] Ch. Jungen, *Elements of Quantum Defect Theory*, edited by M. Quack and F. Merkt, Handbook of High Resolution Spectroscopy, (Wiley, Chichester and New York, 2011), pp. 471-510.

[15] M. Roudjane, F. Launay, and W.-Ü. L. Tchang-Brillet, J. Chem. Phys. **125**, 214305-1 - 214305-9 (2006).

[16] M. Glass-Maujean *et al.* (in preparation).

[17] M. Glass-Maujean, Ch. Jungen, G. Reichardt, A. Balzer, H. Schmoranzer, A. Ehresmann, I. Haar, and P. Reiss, Phys. Rev. **A 82**, 062511-1 - 062511-13 (2010).

[18] R. S. Berry, J. Chem. Phys. **45**, 1228-1245 (1966).

[19] Ch. Jungen and S. T. Pratt, J. Chem. Phys. **133**, 214303-1 - 214303-9 (2010).

[20] G. Herzberg and Ch. Jungen, J. Mol. Spectrosc. **41**, 425-486 (1972).

[21] R. S. Mulliken, J. Am. Chem. Soc. **88**, 1849-1861 (1966).

[22] M. Glass-Maujean, Ch. Jungen, A. Spielfiedel, H. Schmoranzer, I. Tulin, A. Knie, P. Reiss, and A. Ehresmann, J. Mol. Spectrosc. **293-294**, 1-10 (2013).

[23] J. Liu, D. Sprecher, Ch. Jungen, W. Ubachs, and F. Merkt, J. Chem. Phys. **132**, 154301-1 - 154301-11 (2010).

[24] H. Bredohl and G. Herzberg, Can. J. Phys. **51**, 867-887 (1973).

Table 1. $Q(N'')$ absorption transitions to the $4p\pi$, $5p\pi$, $6p\pi$ and $7p\pi$ $^1\Pi_u^-$ levels of D_2

	v	$Q(1)$ [a] observed	o-c	± [b]	$Q(2)$ observed	o-c	±	$Q(3)$ observed	o-c	±	$Q(4)$ observed	o-c	±
$4p\pi$	0	118129.10	-0.23	0.03	118068.85	-0.08	0.03	117978.74	-0.17	0.08	*117859.60*[c]	*-0.10*	*0.60*[d]
$4p\pi$	1	119715.46	-0.21	0.08	119652.99	-0.10	0.03	119559.75	-0.03	0.05	119436.42	0.32	0.05
$4p\pi$	2	121236.81	-0.17	0.03	121172.20	-0.09	0.03	121075.71	-0.06	0.04	120947.86	0.03	0.05
$4p\pi$	3	122694.71	-0.15	0.03	122628.01	-0.07	0.03	122528.35	-0.07	0.04	122396.31	0.00	0.04
$4p\pi$	4	124090.48	-0.15	0.03	124021.74	-0.06	0.03	123918.94	-0.13	0.06	123782.74	-0.13	0.05
$4p\pi$	5	125425.59	-0.09	0.14	125354.80	-0.03	0.04	125249.04	-0.03	0.05	125108.87	0.00	0.10
$4p\pi$	6	126700.76	-0.10	0.04	126628.01	-0.02	0.04	126519.27	-0.05	0.06	*126375.16*	*0.44*	*0.60*
$4p\pi$	7	127917.24	-0.11	0.04	127842.53	-0.03	0.04	127730.78	-0.16	0.05	*127582.92*	*0.38*	*0.60*
$4p\pi$	8	129077.08	-0.15	0.04	129000.64	-0.04	0.04	*128886.42*	*0.48*	*0.60*	128734.97	0.23	0.60
$4p\pi$	9	130168.41	0.15	0.04	130091.13	1.14	0.04	129972.96	-0.02	0.04	*129817.74*	*0.46*	*0.60*
$4p\pi$	10	131213.52	-0.28	0.04	131133.52	-0.07	0.05	*131013.31*	*0.39*	*0.60*	130853.78	1.12	0.60
$4p\pi$	11	132199.20	-0.53	0.05	132116.79	-0.44	0.05	*131994.04*			131830.70		
$4p\pi$	12	133126.63	-1.00	0.05	133042.34	-0.90	0.08	*132917.01*			132749.75		
$4p\pi$	13	133994.03	-3.65	0.05	133907.33	-3.94	0.07	*133782.21*			133611.11		
$4p\pi$	14	134805.23	-4.72	0.11	*134721.68*			*134590.22*			134413.33		
$4p\pi$	15	135565.19	1.84	0.15	135470.23	-2.90	0.4						
$4p\pi$	16	136251.76	0.90	0.5	*136158.82*								
$5p\pi$	0	120466.02	-0.10	0.03	120405.48	-0.08	0.07	120315.23	-0.06	0.10	120195.63	0.37	0.60
$5p\pi$	1	122047.82	-0.11	0.03	121985.01	-0.17	0.03	121891.42	-0.21	0.05	121767.77	0.16	0.04
$5p\pi$	2	123564.82	-0.07	0.04	123499.75	-0.30	0.03	123403.04	-0.25	0.06	123274.92	-0.12	0.06
$5p\pi$	3	125018.67	-0.11	0.04	124949.56	-2.29	0.07	124851.78	-0.20	0.06	124719.58	0.22	0.60
$5p\pi$	4	126411.07	-0.08	0.05	126342.49	0.30	0.04	*126239.29*	*-0.09*	*0.60*	126102.87		
$5p\pi$	5	127744.43	-0.10	0.04	127673.77	0.10	0.05	*127567.93*	*-0.53*	*0.60*	127427.77	-0.17	0.60
$5p\pi$	6	128992.37	0.00	0.05	128920.63	0.25	0.04	128812.76	-0.14	0.08	128670.41		
$5p\pi$	7	130222.32	-0.03	0.04	130147.55	0.11	0.05	*130035.10*			129886.73		
$5p\pi$	8	131376.85	0.04	0.04	131299.49	-0.50	0.07	*131185.30*			131033.21		
$5p\pi$	9	132474.80	0.02	0.05	132396.34	0.23	0.06	*132278.58*			132122.68		
$5p\pi$	10	133516.31	0.05	0.05	133435.89	0.26	0.05	*133315.24*			133155.58		
$5p\pi$	11	134493.13	-0.60	0.07	134412.23	0.12	0.06	*134289.81*			134127.13		
$5p\pi$	12	135425.62	-0.01	0.07	135340.86	-0.05	0.13						
$5p\pi$	13				136214.67	-0.60	0.3						
$5p\pi$	14				137023.65	-0.92	0.13						
$6p\pi$	0	121747.78	-0.14	0.04	121687.21	-0.06	0.05	*121596.89*	*0.11*	*0.60*	121476.24	-0.85	0.10
$6p\pi$	1	123326.19	-0.20	0.03	123263.49	-0.10	0.04	123169.81	-0.11	0.07	123045.61	-0.16	0.10
$6p\pi$	2	124840.04	-0.16	0.07	124775.18	-0.09	0.04	124678.26	-0.13	0.07	*124549.97*	*0.03*	*0.60*
$6p\pi$	3	126290.18	-0.22	0.05	126223.34	-0.01	0.04	126123.26	-0.05	0.05	*125990.69*	*0.21*	*0.60*
$6p\pi$	4	127677.05	-0.15	0.04	127608.14	0.01	0.06	127504.76	0.02	0.05	*127367.77*	*0.53*	*0.60*
$6p\pi$	5	*129029.50*			*128957.47*			128850.11			128707.85		
$6p\pi$	6	130280.95	0.26	0.07	130208.06	-0.17	0.12	*130099.93*			129956.37		
$6p\pi$	7	131494.69	0.45	0.05	131418.69	-0.64	0.07	*131307.91*			131158.26		
$6p\pi$	8	132647.41	0.47	0.05	132568.56	-1.49	0.07	*132455.24*			132303.01		
$6p\pi$	9	133743.59	0.52	0.05	133659.48	-4.79	0.07	*133546.62*			133390.61		
$6p\pi$	10	134782.81	0.48	0.05	134704.88	3.38	0.06	*134580.46*					
$6p\pi$	11	135766.37	0.63	0.06	135685.48	2.31	0.08						
$6p\pi$	12				136610.67	1.63	0.08						
$6p\pi$	13				137479.59	1.97	0.10						
$7p\pi$	0	122526.80	-0.20	0.07	122466.22	-0.10	0.08	*122375.87*					
$7p\pi$	1	124104.92	-0.12	0.10	124042.17	-0.06	0.09	123948.14	-0.37	0.06			
$7p\pi$	2	125617.94	-0.12	0.05	125553.04	-0.08	0.05	*125456.21*					
$7p\pi$	3	127068.71	-0.16	0.04	127001.82	-0.09	0.05	*126902.03*					
$7p\pi$	4	128456.22	-0.19	0.04	128387.26	-0.09	0.05	*128284.27*					
$7p\pi$	5	129784.70	-0.26	0.04	129713.79	-0.12	0.05	*129607.85*					
$7p\pi$	6	131051.74	-0.31	0.07	130978.93	-0.14	0.07	*130870.14*					
$7p\pi$	7	132262.78	-0.56	0.08	132188.10	-0.24	0.08	*132076.39*					
$7p\pi$	8	133414.76	-1.45	0.06	133338.93	-0.35	0.06	*133224.45*					
$7p\pi$	9	*134521.45*			*134434.73*			*134316.93*					
$7p\pi$	10	135555.51	3.20	0.07	135470.22	-0.95	0.08						

[a] The positions of the upper state energy levels above the $v'' = 0$, $N'' = 0$ ground state level are obtained by adding the ground-state rotational energies 59.78 ($N'' = 1$) [23], 179.01 ($N'' = 2$) [24], 357.25 ($N'' = 3$) [24], or 593.64 ($N'' = 4$) [24] cm^{-1}, respectively, to the transition energies.

[b] The columns with headings ± contain the experimental uncertainty for each observed transition (cf. the text).

[c] Transition energies in italics are calculated values.

[d] o-c values and uncertainties in italics correspond to levels observed in Refs. [2, 3] but not observed in the present work. The energy given in these cases is the calculated value.

Table 2. $Q(N'')$ absorption transitions to the $np\pi$ ($n = 8 - 14$) $^1\Pi_u^-$ levels of D$_2$

	v	$Q(1)$ [a] observed	o-c	± [b]	$Q(2)$ observed	o-c	±
$8p\pi$	0	123034.87[c]	1.23	0.60[d]	122974.08	-0.09	0.09
$8p\pi$	1	124611.95	-0.07	0.04	124549.36	0.08	0.09
$8p\pi$	2	126124.24	-0.17	0.12	126059.45	-0.05	0.05
$8p\pi$	3	127573.14	-0.10	0.04	127506.21	-0.07	0.04
$8p\pi$	4	128959.28	-0.09	0.05	128889.98	-0.15	0.05
$8p\pi$	5	130296.65			130224.82		
$8p\pi$	6	131559.37	-0.17	0.07	131486.34	-0.12	0.08
$8p\pi$	7	132768.61	-0.36	0.07	132693.76	-0.23	0.09
$8p\pi$	8	133920.62	-0.46	0.05	133843.80	-0.36	0.08
$8p\pi$	9	135015.61	-0.73	0.06	134937.20	-0.33	0.08
$8p\pi$	10				136955.00	-1.15	0.10
$9p\pi$	0	123384.86	1.14	0.60	123324.13	2.27	0.60
$9p\pi$	1	124961.56	-0.12	0.09	124898.83		
$9p\pi$	2	126473.74	-0.18	0.07	126408.86	-0.07	0.12
$9p\pi$	3	127922.83	-0.20	0.11	127855.84	-0.11	0.10
$9p\pi$	4	129310.36	-0.15	0.07	129241.29	-0.11	0.30
$9p\pi$	5	130637.45	-0.22	0.08	130566.45	-0.41	0.16
$9p\pi$	6	131905.58	-0.14	0.08	131832.37	-0.09	0.12
$9p\pi$	7	133114.90	-0.26	0.07	133040.10	-0.14	0.06
$9p\pi$	8	134267.72	-0.32	0.08	134191.90		
$9p\pi$	9	135362.24	-0.41	0.07	135283.74	-0.15	0.10
$10p\pi$	0	123635.42	1.48	0.60	123574.42	-0.33	0.11
$10p\pi$	1	125212.38	0.29	0.12	125149.10	-0.14	0.15
$10p\pi$	2	126723.94	-0.13	0.07	126658.97	-0.11	0.08
$10p\pi$	3	128172.81	-0.15	0.06	128105.86	-0.02	0.07
$10p\pi$	4	129560.51	0.29	0.09	129491.04	-0.07	0.08
$10p\pi$	5	130886.94	-0.21	0.09	130816.00	-0.02	0.20
$10p\pi$	6	132154.71	-0.11	0.09	132081.47	-0.25	0.09
$10p\pi$	7	133363.81	-0.23	0.22	133288.92	-0.07	0.16
$11p\pi$	0	123821.46	1.34	0.60	123760.79	1.31	0.60
$11p\pi$	1	125397.89	-0.05	0.07	125335.08	1.52	0.60
$11p\pi$	2	126909.64	-0.09	0.06	126844.59	-0.13	0.23
$11p\pi$	3	128358.25	-0.14	0.06	128291.27	-0.03	0.07
$11p\pi$	4	129745.07	-0.12	0.07	129675.99	-0.05	0.11
$11p\pi$	5	131073.73			131002.50		
$11p\pi$	6	132340.57			132267.47		
$11p\pi$	7	133549.66	-0.29	0.14	133474.90		
$11p\pi$	8	134701.86			134624.83	-0.08	0.12
$12p\pi$	0	123963.25	2.55	0.60	123902.57	0.13	0.60
$12p\pi$	1	125539.38	-0.19	0.06	125476.70		
$12p\pi$	2	127050.64	-0.08	0.06	126985.57	-0.06	0.08
$12p\pi$	3	128500.30	-0.06	0.07	128433.25		
$12p\pi$	4	129887.16	-0.08	0.11	129818.06	-0.05	0.11
$12p\pi$	5	131214.31			131142.82		
$12p\pi$	6	132481.68			132408.50		
$12p\pi$	7	133690.58	-0.23	0.06	133615.76		
$12p\pi$	8	134842.85	-0.19	0.20	134766.08		
$13p\pi$	0	124073.72	1.48	0.60	124013.03	1.37	0.60
$13p\pi$	1	125650.89	1.01	0.60	125587.52		
$13p\pi$	2	127161.70	-0.15	0.12	127096.84		
$13p\pi$	3	128610.21	-0.19	0.09	128543.30		
$13p\pi$	4	129997.10	-0.26	0.06	129928.20	-0.03	0.11
$13p\pi$	5	131323.85	-0.17	0.13	131252.89		
$13p\pi$	6	132591.33	-0.18	0.12	132518.41		
$13p\pi$	7	133800.98	-0.01	0.15	133725.95		
$13p\pi$	8	134952.74	-0.12	0.15	134875.90		
$14p\pi$	0	124161.71	1.09	0.60	124101.03		
$14p\pi$	1	125737.95			125675.08	1.12	0.60
$14p\pi$	2	127249.51	1.29	0.60	127184.50		
$14p\pi$	3	128697.94	-0.08	0.10	128630.92		
$14p\pi$	4	130084.70	-0.24	0.06	130015.80		
$14p\pi$	5	131411.37	-0.21	0.14	131340.43		
$14p\pi$	6	132679.13	-0.03	0.14	132606.04		
$14p\pi$	7	133887.94	-0.31	0.15	133813.20		
$14p\pi$	8	135040.21	-0.50	0.20	134963.72		

[a] The positions of the upper state energy levels above the $v'' = 0, N'' = 0$ ground state level are obtained by adding the ground-state rotational energies 59.78 ($N'' = 1$) [23], or 179.01 ($N'' = 2$) [24] cm^{-1}, respectively, to the transition energies.

[b] The columns with headings ± contain the experimental uncertainty for each observed transition (cf. the text).

[c] Transition energies in italics are calculated values.

[d] o-c values and uncertainties in italics correspond to levels observed in Refs. [2, 3] but not observed in the present work. The energy given in these cases is the calculated value.